

Investigation of photoneutron reactions close to and above the neutron emission threshold in the rare earth region

J. Hasper,¹ S. Müller,¹ D. Savran,¹ L. Schnorrenberger,¹ K. Sonnabend,¹ and A. Zilges^{1,2}

¹ *Institut für Kernphysik, Technische Universität Darmstadt,*

Schlossgartenstraße 9, D-64289 Darmstadt

² *Institut für Kernphysik, Universität zu Köln,*

Zülpicher Straße 77, D-50937 Köln

(Dated: February 2, 2008)

Abstract

We have investigated the photoneutron cross section of the isotopes $^{148,150}\text{Nd}$, ^{154}Sm , and $^{154,160}\text{Gd}$ close to the neutron emission threshold in photoactivation experiments at the Darmstadt superconducting electron linear accelerator S-DALINAC. Naturally composed targets were activated with a high-intensity bremsstrahlung beam at various energies and the reaction yields have been determined by measuring the activity of the produced radioactive isotopes with HPGe detectors. The results are compared to two different statistical model calculations.

PACS numbers: 25.20.-x, 26.20.+f, 26.30.+k

Keywords: nucleosynthesis, photoactivation, photodisintegration, bremsstrahlung, rare earth nuclei

I. INTRODUCTION

The nucleosynthesis of the elements heavier than iron is dominated by the slow neutron capture process (s process) and the rapid neutron capture process (r process). However, 35 proton-rich stable isotopes cannot be produced in either of these two processes and are believed to be mainly synthesized by a combination of photodisintegration reactions, i. e. (γ, n) , (γ, p) and (γ, α) reactions, in the explosive scenario of the p process [1, 2]. An accurate description of the nucleosynthesis within these processes demands reliable input from nuclear physics.

Calculations of astrophysical reaction networks within the p process have to account for a huge number of reaction rates. Many of the isotopes involved in the network are off the valley of stability and, therefore, are not accessible by experiments in many cases. But even for the stable nuclei experimental data for photodisintegration reactions in the astrophysically relevant energy region, i. e. close to the particle emission threshold, are rare. Hence, the reaction rates mainly need to be adopted from theoretical predictions. It is mandatory to test the predictive power of the calculations for those isotopes, which can be studied in the laboratory, and to prove the reliability of the predictions for the extrapolation to unstable nuclei.

The situation is much better for the s process. Since for the unstable isotopes within the s -process reaction network the β -decay rate usually highly exceeds the neutron capture rate, the reaction path follows the valley of stability and, hence, mainly stable isotopes are involved. Therefore, extensive experimental studies have been carried out in neutron capture experiments in the last decades and neutron capture cross sections for a wide range of isotopes have become available with uncertainties of only a few percent [3, 4]. With this enormous amount of nuclear physics input the understanding of s -process nucleosynthesis and its astrophysical sites has largely improved. However, for some unstable isotopes along the reaction path, the so-called *branching points*, β -decay and neutron capture become competitive. Since the branching ratio of β -decay and neutron capture is highly sensitive to the physical conditions, e. g. temperature and neutron density, in the stellar environment during the s process, these branching points serve as an excellent test for s -process nucleosynthesis models. Thus, it is essential to determine the neutron capture cross sections of these isotopes with high accuracy. Unfortunately, due to their short half-life

neutron capture experiments can hardly be performed and, hence, further improvements of nucleosynthesis models are still hampered by the relatively large uncertainties of the cross section predictions for these isotopes [5]. Nevertheless, information for the neutron capture cross sections of branching points can be derived from studying the (γ, n) reaction of the stable neighbouring nucleus. The idea to determine (n, γ) reaction rates via photodisintegration experiments has already been presented in [6].

Experiments with real photons provide a well-suited tool to study photodisintegration cross sections and ground-state reaction rates. In previous experiments we have concentrated our investigations on isotopes of mass $A \geq 186$ and confirmed the validity of several theoretical predictions in this mass region [6, 7, 8, 9, 10]. Average deviations between experiment and theory were typically less than 30%.

In this paper we want to address the photodisintegration reactions in the rare earth region (see Fig. 1). This region is of particular interest for the s process, because the isotopic abundance pattern is shaped by several branchings at the unstable isotopes of Nd, Pm, Sm, Eu and Gd. Since the relative abundances of the involved isotopes are known with an uncertainty of better than two percent [11], this mass region is exceptionally suited to test the stellar nucleosynthesis models with high accuracy. To provide precise nuclear physics input, neutron capture cross sections of several branching points have been measured with high accuracy in the last years [12, 13, 14, 15]. But still one has to rely on theoretical predictions of the cross sections of short-lived branching points, e. g. ^{147}Nd and ^{153}Gd . Therefore, we have investigated the inverse photoneutron reactions of ^{148}Nd and ^{154}Gd in order to improve the reliability of these predictions.

Furthermore, the abundances of some isotopes in this region receive large contributions from the p process, e. g. a 33% contribution is predicted for ^{152}Gd [11]. For a comprehensive description of the nucleosynthesis in this mass region these contributions cannot be neglected and need to be studied in detail. Hence, the aim of this work is also to provide reliable data for the photoneutron reaction rates of some selected isotopes to prove the predictive power of the theoretical calculations in this mass region.

We have performed photoactivation experiments to study the (γ, n) reactions of the isotopes $^{148,150}\text{Nd}$, ^{154}Sm and $^{154,160}\text{Gd}$ in the astrophysically relevant energy region close to the neutron emission threshold at the superconducting Darmstadt electron linear accelerator

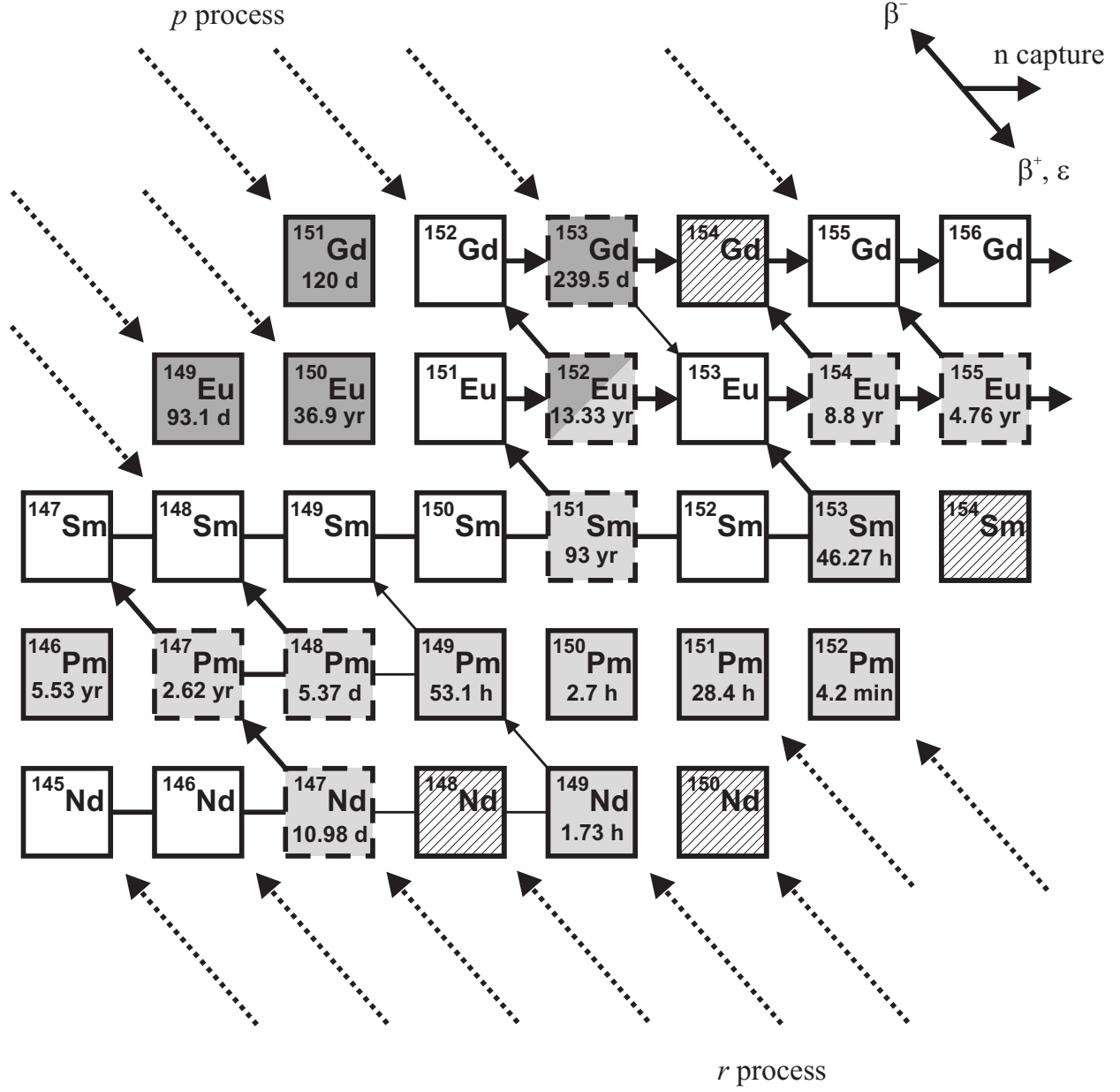


FIG. 1: The s -process flow (solid lines) in the rare earth region. The thickness of the solid lines indicates the strength of the reaction flow. The reaction path is influenced by several branching points (dashed boxes). Unstable isotopes are shaded light grey (β^-) and dark grey (β^+, ϵ). Most isotopes also have nucleosynthesis contributions from the r and p process (dotted lines), respectively. The photoneutron reactions of the hatched isotopes have been studied in this work.

S-DALINAC [16]. Our experimental setup is discussed in detail in Sec. II. We explain the data analysis and the approach to derive astrophysically relevant ground-state reaction rates directly from the experiment by approximating a thermal Planck spectrum by a superposition of different bremsstrahlung spectra in Sec. III. The results are presented in Sec. IV and compared to two theoretical calculations based on the framework of the Hauser-Feshbach theory.

II. EXPERIMENTAL SETUP

We have irradiated naturally composed neodymium, gadolinium and samarium targets at the superconducting electron linear accelerator S-DALINAC. The experimental setup is illustrated in Fig. 2. A monoenergetic electron beam of energy E_0 is stopped completely in a thick copper radiator and produces a continuous spectrum of bremsstrahlung photons with a maximum energy of $E_{\max} = E_0$. The photons irradiate the target, which is mounted directly behind the radiator. Thin metallic discs ($m = 40 - 50$ mg) were used as neodymium and gadolinium targets, whereas samarium was available as pressed pills of Sm_2O_3 powder ($m = 500 - 1750$ mg). Each target had a diameter of 20 mm. The target specifications are summarized in Tab. I.

The photon flux intensity was determined by observing the photon scattering reaction $^{11}\text{B}(\gamma, \gamma')$ behind a copper collimator system with actively-shielded high-purity germanium (HPGe) detectors. To compare the photon flux intensity at the target position in front of the collimator and at the position of the $^{11}\text{B}(\gamma, \gamma')$ target behind the collimator thin metallic rhenium discs have been irradiated simultaneously at both positions to normalize the photon flux intensity via the photodisintegration reaction $^{187}\text{Re}(\gamma, n)$, which was studied in [10]. A detailed discussion of the photon flux calibration is given in the following section.

The advantage of irradiating the targets in front of the collimator becomes clear from Fig. 3. At this position the much more intense photon flux guarantees a high reaction yield for the irradiation even for small amounts of target material and small photodisintegration cross sections.

The irradiation was performed at various energies E_{\max} starting just above the neutron emission threshold of $^{148,150}\text{Nd}$ with $E_{\max} = 7450$ keV. The energy was increased in steps of 150 and 200 keV up to $E_{\max} = 9800$ keV. The duration of each activation run was between

Isotope	Form	Abundance [%]	Weight [mg]	S_n [keV]	Analyzed γ -transition [keV]	I_γ [%]
^{148}Nd	metal foil	5.76	40-50	7332.9	91.1	27.9 ± 1.1
					531.0	13.1 ± 0.9
^{150}Nd	metal foil	5.64	40-50	7379.9	114.3	19.2 ± 1.5
					155.9	5.93 ± 0.31
					211.3	25.9 ± 1.4
					267.7	6.03 ± 0.28
					270.1	10.6 ± 0.5
^{154}Gd	metal foil	2.18	40-50	8894.8	97.4	29.0 ± 0.8
					103.2	21.1 ± 0.6
^{160}Gd	metal foil	21.86	40-50	7451.4	58.0	2.49 ± 0.07
					226.0	0.217 ± 0.002
					348.3	0.239 ± 0.003
					363.6	11.8 ± 0.1
^{154}Sm	oxide	22.70	500-1750	7967.6	69.7	4.73 ± 0.04
					97.4	0.772 ± 0.019
					103.2	29.3 ± 0.2
^{187}Re	metal foil	62.60	320-340	7363.0	122.6	0.603 ± 0.003
					137.2	9.47 ± 0.30

TABLE I: Specifications of targets and calibration targets used for the activation experiments. The intensities per decay I_γ were taken from [17].

6 and 24 hours.

A. Calibration of photon flux

The spectral distribution of the photon flux is taken from a simulation using the Monte Carlo code GEANT4 [18]. The absolute normalization of the photon flux intensity can be derived from the reaction yields of the photodisintegration reaction $^{187}\text{Re}(\gamma, n)$ and the photon scattering reaction $^{11}\text{B}(\gamma, \gamma')$, respectively.

The reaction yield $Y_{(\gamma, n)}^{E_{\text{max}}}$ of the photoactivation using bremsstrahlung with a maximum energy E_{max} is given by:

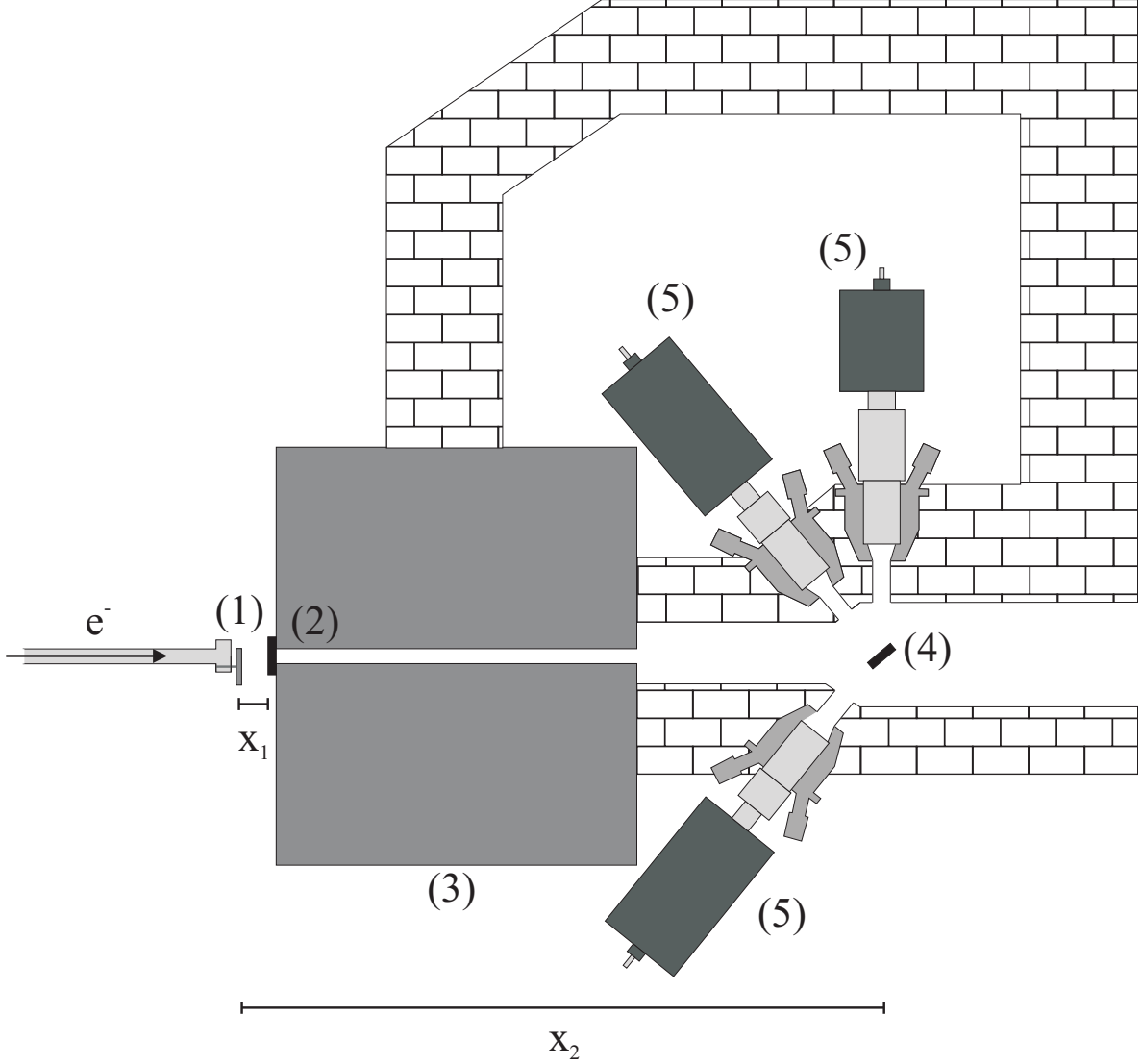


FIG. 2: Schematic layout of the photoactivation setup. A monoenergetic electron beam produces bremsstrahlung in a massive copper radiator with a thickness of 1.2 cm (1). The photons activate the target of interest ($x_1 \approx 5$ cm), which is sandwiched between several calibration targets (2). Behind a thick copper collimator system (3) a boron target (4) is mounted ($x_2 \approx 150$ cm) to monitor the photon flux via the photon scattering reaction $^{11}\text{B}(\gamma, \gamma')$ with actively-shielded HPGe detectors (5).

$$Y_{(\gamma,n)}^{E_{\max}} = N_T \int N_\gamma(E, E_{\max}) \sigma_{(\gamma,n)}(E) dE, \quad (1)$$

where N_T denotes the number of target nuclei, $N_\gamma(E, E_{\max})$ the time-integrated photon flux $\int_0^{t_{\text{act}}} n_\gamma(E, E_{\max}, t) dt$ for the duration of activation t_{act} and $\sigma_{(\gamma,n)}$ is the photoneutron

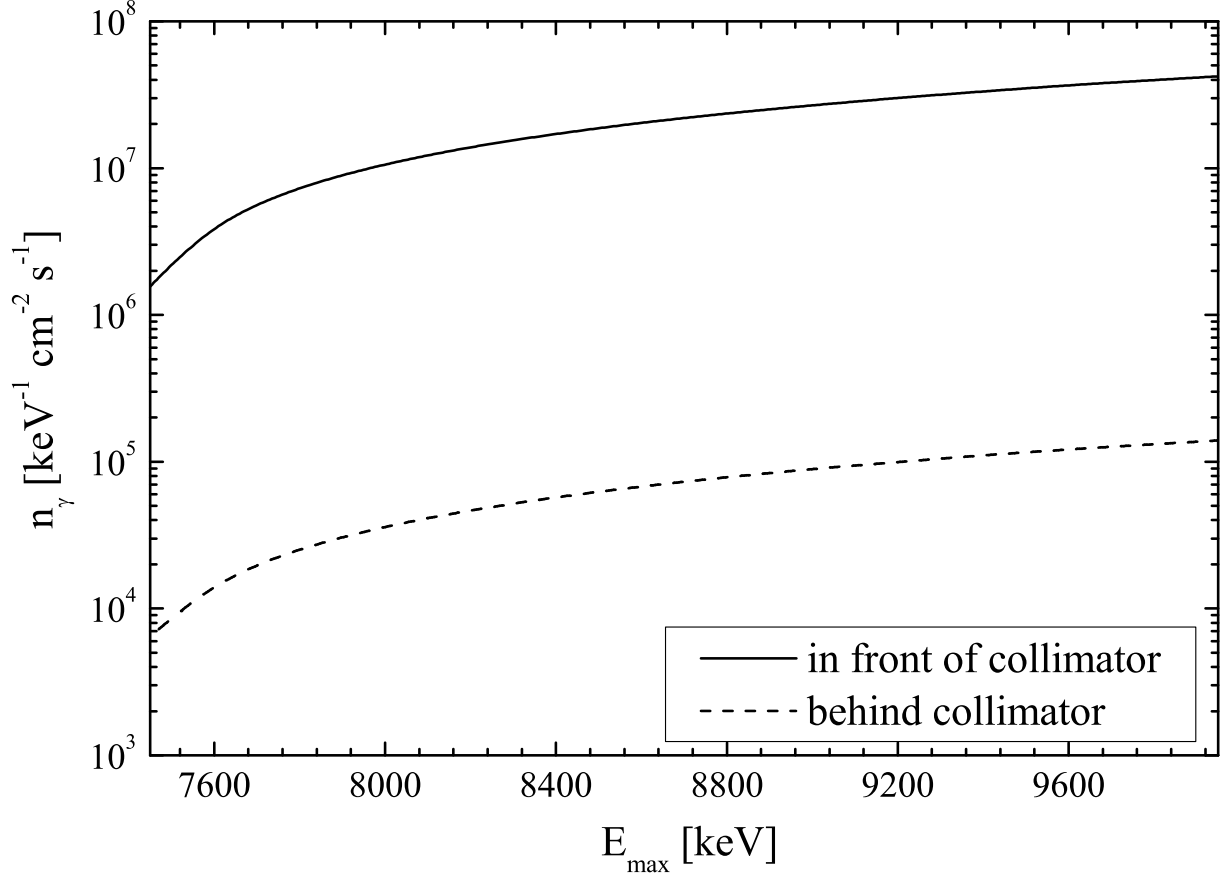


FIG. 3: Available photon flux n_γ at our photoactivation setup for a photon energy of $E_\gamma = S_n(^{148}\text{Nd}) = 7332.9$ keV as a function of the maximum photon energy of the spectral distribution E_{max} . A mean electron current of $I_e = 25$ μA on the radiator has been assumed. The photon flux was obtained from a simulation using the Monte Carlo code GEANT4 [18] and confirmed experimentally by the two approaches discussed in the text. The photon flux in front of the collimator is about 270 times more intense than behind the collimator and the energy dependence is nearly equal.

cross section. Using a simulation $N_{\gamma,\text{sim}}(E, E_{\text{max}})$ for the spectral distribution of the photon flux the normalization factor $N_{\gamma,0}^{E_{\text{max}}}$ for the simulation can then be derived from:

$$N_{\gamma,0}^{E_{\text{max}}} = \frac{Y_{(\gamma,n)}^{E_{\text{max}}}}{N_T \int N_{\gamma,\text{sim}}(E, E_{\text{max}}) \sigma_{(\gamma,n)}(E) dE}. \quad (2)$$

By irradiating ^{187}Re both in front and behind the collimator one can determine the normalization for the photon flux intensity at both target positions from the well-known

photoneutron cross section of ^{187}Re and the measured reaction yield $Y_{(\gamma,n)}^{E_{\max}}$.

A second approach for the normalization is to observe the photon scattering reaction $^{11}\text{B}(\gamma, \gamma')$ with HPGe detectors behind the collimator. The reaction yield for a certain transition from a state of energy E_i into a state of energy E_j is given by:

$$Y_{i \rightarrow j} = N_{\text{Bor}} \cdot N_{\gamma}(E_i, E_{\max}) \cdot I_{i \rightarrow j} , \quad (3)$$

where N_{Bor} is the number of ^{11}B nuclei in the target and $I_{i \rightarrow j}$ denotes the integrated cross section of the observed γ -transition. With the knowledge of $I_{i \rightarrow j}$ one can directly determine the photon flux intensity at various energies by observing different transitions. These data points can then be used for the normalization of the full photon spectrum. Figure 4 shows the normalized photon flux distribution calculated with GEANT4 in comparison to the experimental data points of the $^{11}\text{B}(\gamma, \gamma')$ reaction. A mean deviation of 10% to 20% between simulation and experimental data was found depending on the maximum photon energy E_{\max} . In comparison with former simulations using GEANT3 [19] the shape of the photon flux is correctly described by GEANT4 and, therefore, a correction procedure of the shape of the simulated photon flux distribution close to E_{\max} [7] does not need to be applied anymore. This proves the reliability of the simulation.

Nevertheless, this approach only yields the normalization of the photon flux intensity at the target position behind the collimator, but we assumed that the same normalization factor was valid at the target position in front of the collimator. In addition, to confirm the normalization based on the $^{11}\text{B}(\gamma, \gamma')$ reaction the photon flux intensity was derived from the photodisintegration reaction $^{187}\text{Re}(\gamma, n)$ at both target positions. As seen from Fig. 5 both approaches are in excellent agreement.

B. Determination of reaction yield

In order to determine the reaction yield $Y_{(\gamma,n)}$, i. e. the number of (γ, n) -reactions occurring during the irradiation, the γ -transitions following the β -decays of the produced unstable isotopes were measured offline with HPGe detectors after the activation. The detectors were covered by thick lead shielding to reduce natural background. The reaction yield is directly proportional to the peak areas of the corresponding γ -transitions in the spectra. The factor of proportionality can be determined with regard to the activation time, the detection effi-

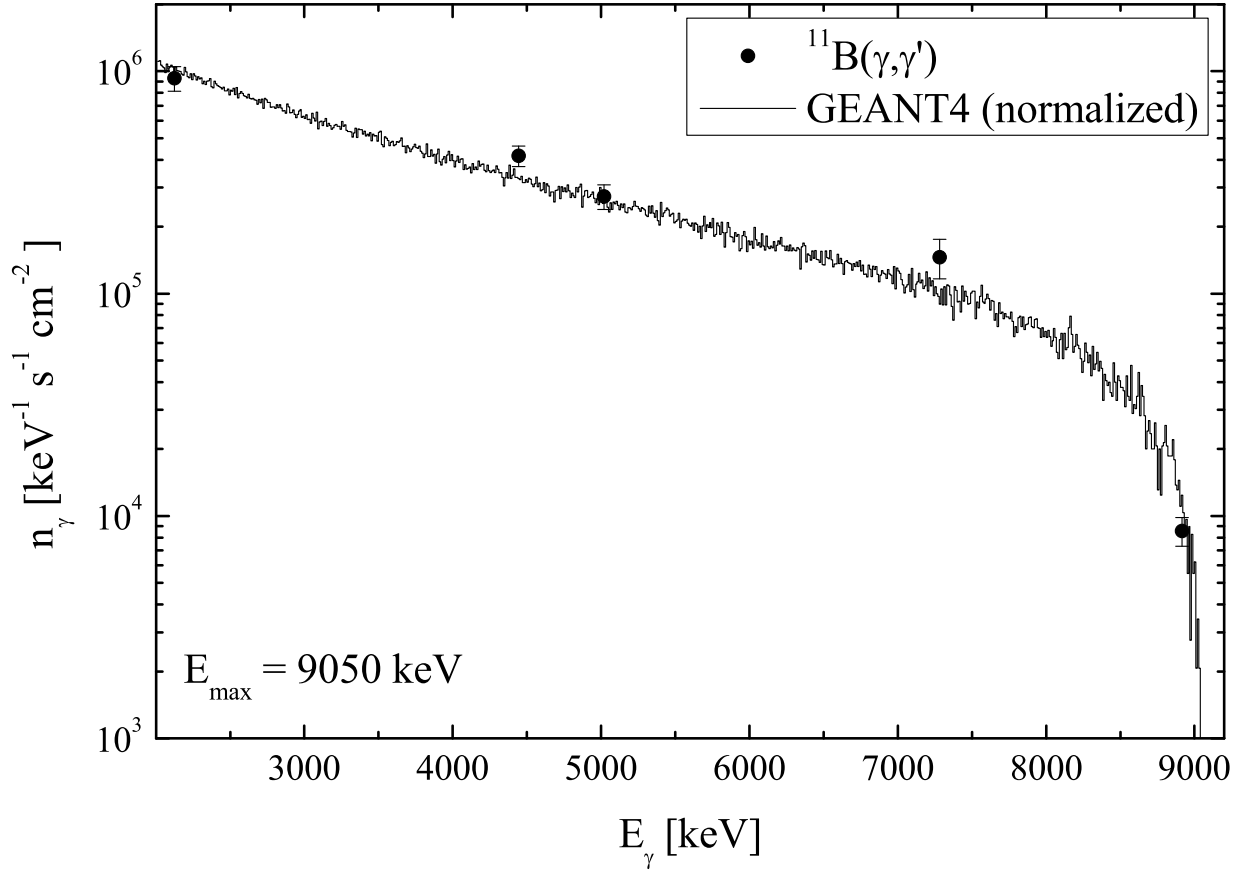


FIG. 4: The simulated photon flux distribution at the target position behind the collimator for $E_{\max} = 9050$ keV. The simulation was normalized to the experimental data obtained from the reaction yields of the photon scattering reaction $^{11}\text{B}(\gamma, \gamma')$ (see text for details).

ciency and the γ -intensities. This has been discussed in detail in [7].

Two different setups have been used to measure the activity of the produced unstable isotopes. One setup consisted of two low-energy photon spectrometers (LEPS), which are highly sensitive to low-energy photons down to a few keV due to a very thin beryllium entrance window. They were positioned face-to-face with a distance of only 10 mm to each other. The targets were mounted directly between the two detectors to obtain a high detection efficiency. Figure 6 shows a spectrum of an irradiated naturally composed neodymium target. Due to the excellent energy resolution of the detectors ($\Delta E_{\gamma}^{\text{FWHM}} \approx 0.5$ keV at $E_{\gamma} = 100$ keV) the observed γ -transitions could be clearly assigned to the corresponding β -decays. However, due to the high detection efficiency, summing effects of coincident γ -rays stemming from the same decay cascade cannot be neglected and have to be carefully cor-

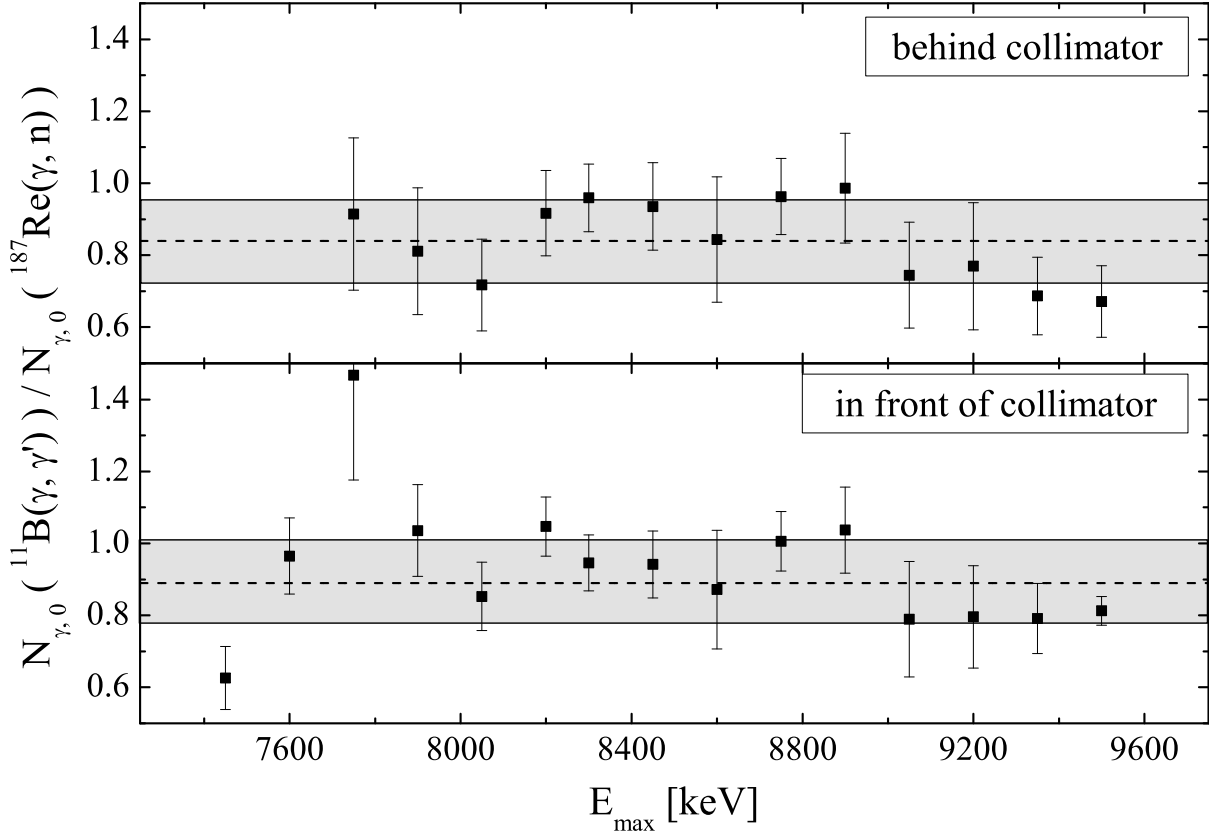


FIG. 5: The ratio of the normalization factors $N_{\gamma,0}$ found for the photon flux intensities at different energies E_{\max} using the reactions ${}^{187}\text{Re}(\gamma, n)$ and ${}^{11}\text{B}(\gamma, \gamma')$, respectively. Both reactions are in good agreement with regard to the experimental error bars and the uncertainty of the photoneutron cross section of ${}^{187}\text{Re}$ (grey error band) [10]. The mean ratio of both approaches is indicated by the dashed line. At $E_{\max} = 7450$ keV and $E_{\max} = 7600$ keV the ${}^{187}\text{Re}(\gamma, n)$ reaction yield was too low to obtain data points behind the collimator.

rected in the analysis of the reaction yield. For the isotopes studied in this work a maximum correction of about 10% was found for the summing of γ -rays and x-rays in the case of the electron capture of ${}^{153}\text{Gd}$.

At the second setup a HPGe detector with 30% efficiency relative to a $3'' \times 3''$ NaI detector was used. Here the targets were mounted at a larger distance of 81 mm in front of the detector. Thus, almost no summing effects occurred in the spectra. However, due to the much smaller detection efficiency this second setup was only used to verify the results obtained at the LEPS setup for a few selected targets.

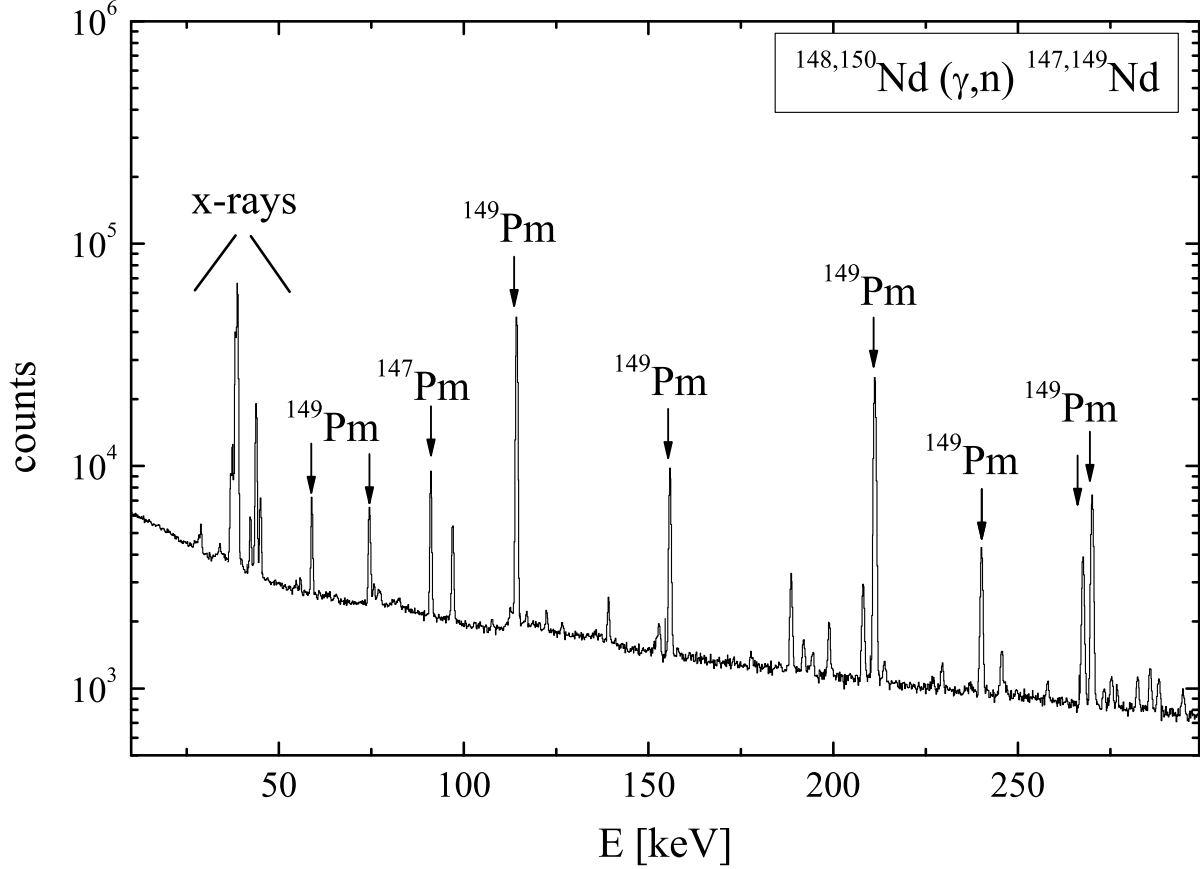


FIG. 6: Typical γ -decay spectrum of a neodymium target irradiated at $E_{\text{max}} = 8600$ keV for a duration of about 13 hours. The spectrum was accumulated over a period of 3 hours at the LEPS setup. The strongest γ -transitions following the β -decays of ^{147}Nd into ^{147}Pm and ^{149}Nd into ^{149}Pm , respectively, are indicated.

To determine the absolute efficiency of our setup, the efficiency of the detectors was simulated in detail using GEANT4. In addition, the efficiencies at certain energies between 14 keV and 1350 keV were measured using standard calibration sources, which served as normalization for the calculated efficiencies. Moreover, a non-calibrated ^{190}Ir source was used to confirm the predicted energy dependence of the efficiency. Figure 7 shows that the normalized simulations are in good agreement with the experimental data points. From the uncertainties of the experimental data points and the deviation of the normalized simulation to these data points, it was estimated that the energy-dependent detection efficiency can be determined with an uncertainty of better than 7% for energies of up to about 1500 keV.

The simulations were also used to account for the self-absorption of the low-energy decay

γ -rays within the target. Whereas the corrections were almost negligible for the very thin neodymium and gadolinium foils, corrections of up to 80% had to be applied for the relatively thick Sm_2O_3 targets. To test the reliability of the simulations the self-absorption was also measured at different photon energies for a variety of targets. Deviations between measurement and simulation were found to be of the order of a few percent.

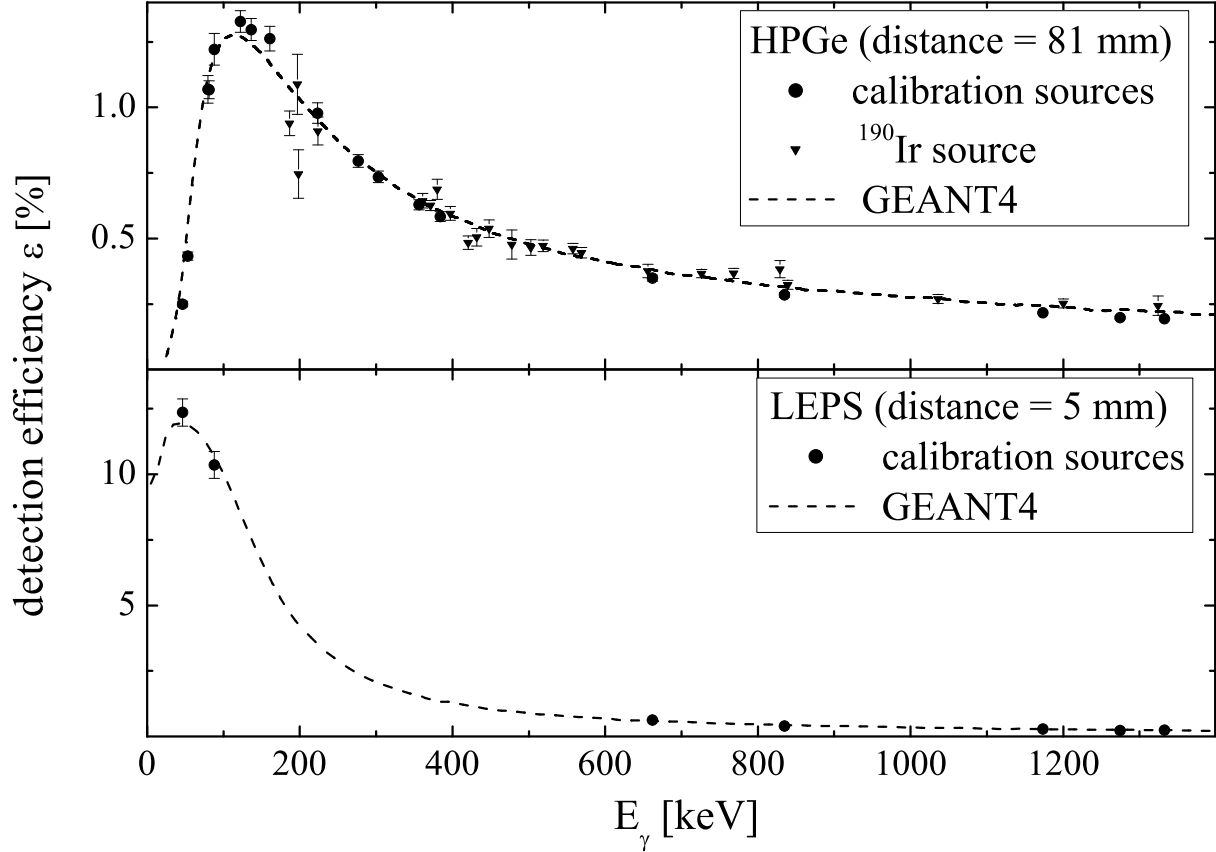


FIG. 7: Absolute detection efficiency of the HPGe and LEPS setup. Standard calibration sources were used to normalize the efficiency curve calculated with GEANT4. Due to large summing effects of coincident γ -rays at small distances between detector and source, only those calibration sources without γ -cascades were used for the normalization in case of the LEPS setup.

III. DATA ANALYSIS

A. Cross section determination

The reaction yield $Y_{(\gamma,n)}^{E_{\max}}$ is directly proportional to the energy-integrated cross section I_σ , which is given by the integral from Eq. (1). Since bremsstrahlung is characterized by a continuous spectral distribution, a deconvolution of the determined integrated cross section I_σ is not possible in general. Therefore, the cross section $\sigma_{(\gamma,n)}$ cannot be derived directly. However, if a theoretical prediction for $\sigma_{(\gamma,n)}$ is adopted, one can calculate I_σ from Eq. (1) and then derive a normalization factor f for the prediction from a comparison to the experimentally determined yields:

$$f(E_{\max}) = \frac{I_\sigma^{\text{Exp}}}{\int_{S_n}^{E_{\max}} N_\gamma(E, E_{\max}) \cdot \sigma_{(\gamma,n)}^{\text{Theory}}(E) dE} . \quad (4)$$

By irradiating at different energies E_{\max} and deriving f for each energy one can test the theoretical prediction for $\sigma_{(\gamma,n)}$ within different energy ranges. If $\sigma_{(\gamma,n)}$ is accurately described, then f should be independent of E_{\max} and close to unity. However, our photoactivation experiments using bremsstrahlung only have limited sensitivity to the shape of $\sigma_{(\gamma,n)}$, since the normalization is an average over a wide energy range as illustrated in Fig. 8.

B. Ground-state reaction rates

The photodisintegration reaction rate λ for a nucleus in a thermal photon bath is given by

$$\lambda(T) = \int_0^\infty n_\gamma^{\text{Planck}}(E, T) \sigma_{(\gamma,n)}(E) dE, \quad (5)$$

where $\sigma_{(\gamma,n)}$ is the photoneutron cross section and n_γ^{Planck} the photon flux per energy interval given by the Planck distribution

$$n_\gamma^{\text{Planck}}(E, T) = c \left(\frac{1}{\pi}\right)^2 \left(\frac{1}{\hbar c}\right)^3 \frac{E^2}{\exp E/kT - 1}. \quad (6)$$

Although it is not possible to produce a thermal photon bath at p -process conditions, i. e. with the intensities resulting from temperatures between 2 and 3×10^9 K, and thus

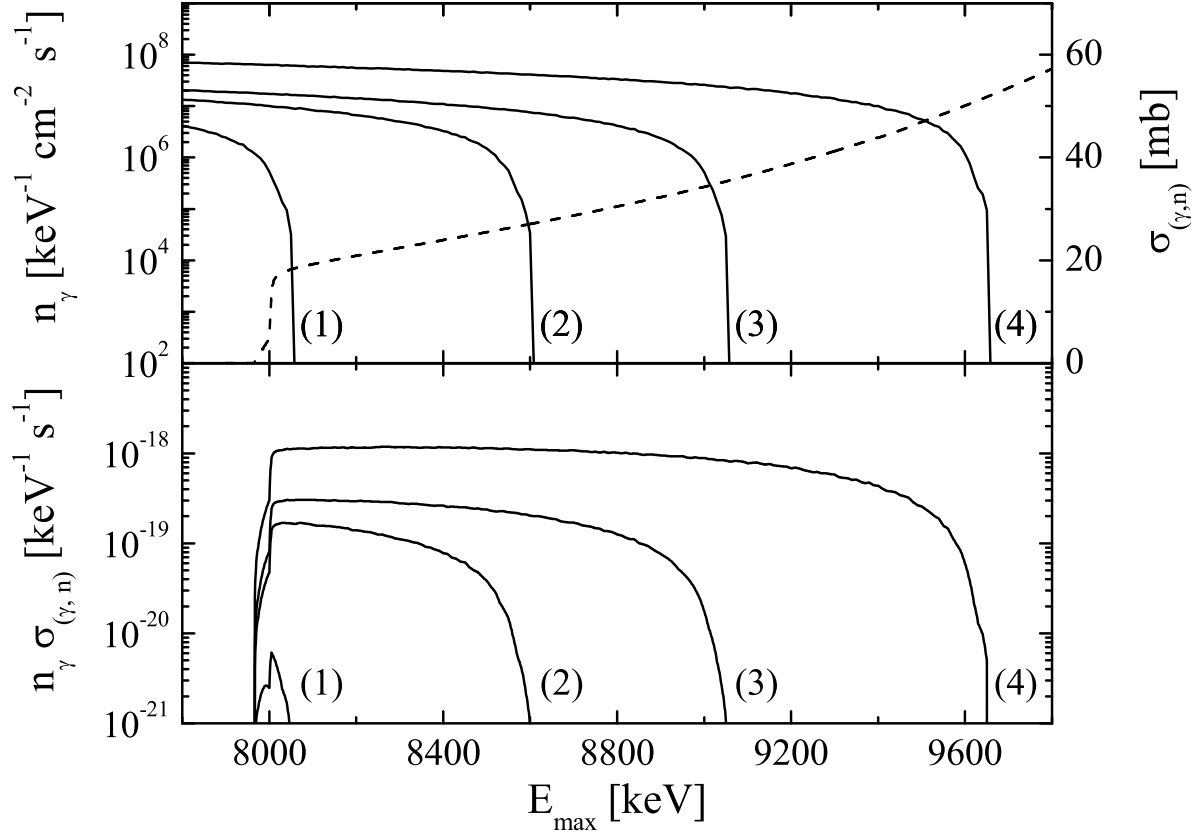


FIG. 8: The top panel shows the simulated spectral distribution of bremsstrahlung at different energies E_{max} of (1) 8050 keV, (2) 8600 keV, (3) 9050 keV and (4) 9650 keV (solid lines) in comparison to the photoneutron cross section $\sigma_{(\gamma,n)}$ of ^{154}Sm (dashed line) predicted by the NON-SMOKER^{WEB} code [20]. The product of $\sigma_{(\gamma,n)}$ and n_γ yields the integrand of Eq. (1), which covers a broad energy range close to the neutron separation energy as shown in the bottom panel.

to measure stellar reaction rates in the laboratory, we can use two different approaches to determine the ground-state reaction rates $\lambda^{\text{g.s.}}$ in the experiment. The obvious way is to use the normalized cross section $\sigma_{(\gamma,n)} = f \cdot \sigma_{(\gamma,n)}^{\text{Theory}}$ from the analysis described in the preceding section and then calculate the integral of Eq. (5). However, using this method one has to rely on the adopted theoretical prediction of the energy dependence of the cross section. This might lead to large systematic uncertainties, if the predicted shape of the cross section deviates significantly from its real shape, e. g. if some resonances above the neutron emission threshold are omitted in the theoretical description. Hence, an approach is preferred where the reaction rates can be directly determined from the experimental data without the need

of any theoretical input. This can be achieved by approximating the Planck spectrum at temperature T with a superposition of several bremsstrahlung spectra $n_{\gamma}^{\text{Brems}}(E, E_{\text{max}}^i)$ at different energies E_{max} [21]

$$n_{\gamma}^{\text{Planck}}(E, T) \approx \sum_i a_i(T) n_{\gamma}^{\text{Brems}}(E, E_{\text{max}}^i), \quad (7)$$

where $a_i(T)$ are temperature-dependent weighting coefficients. With this approximation Eq. (5) can then be written as

$$\lambda(T) \approx \sum_i a_i(T) \int n_{\gamma}^{\text{Brems}}(E, E_{\text{max}}^i) \sigma_{(\gamma,n)}(E) dE \quad (8)$$

$$= \sum_i a_i(T) I_{\sigma,i}^{\text{Exp}}. \quad (9)$$

Since the integrated cross sections $I_{\sigma,i}^{\text{Exp}}$ are directly determined from the experiment the reaction rates can be obtained without further assumptions on the energy dependence of the cross section. Therefore, this analysis is free of systematic uncertainties stemming from the uncertainties of any cross section prediction. The deviation between the approximated and the real Planck spectrum in the relevant energy region for astrophysical studies close to the neutron threshold energy (the so-called *Gamow-like window* [21]) is of the order of 10%, depending on how many bremsstrahlung spectra are used for the approximation (see Fig. 9).

IV. RESULTS

A. Normalization of theoretical predictions

We have determined normalization factors for two different theoretical predictions of the photoneutron cross section $\sigma_{(\gamma,n)}$, which were calculated with the NON-SMOKER^{WEB} code by Rauscher [20] and the TALYS code by Koning *et al.* [22]. Both theoretical predictions are based on the Hauser-Feshbach formalism presuming that the nuclear level density in the energy range close to the neutron threshold is high enough for a statistical treatment. Different results between the two calculations can mainly be ascribed to the nuclear physics input used in the codes, e. g. the neutron optical potential, nuclear level densities and the

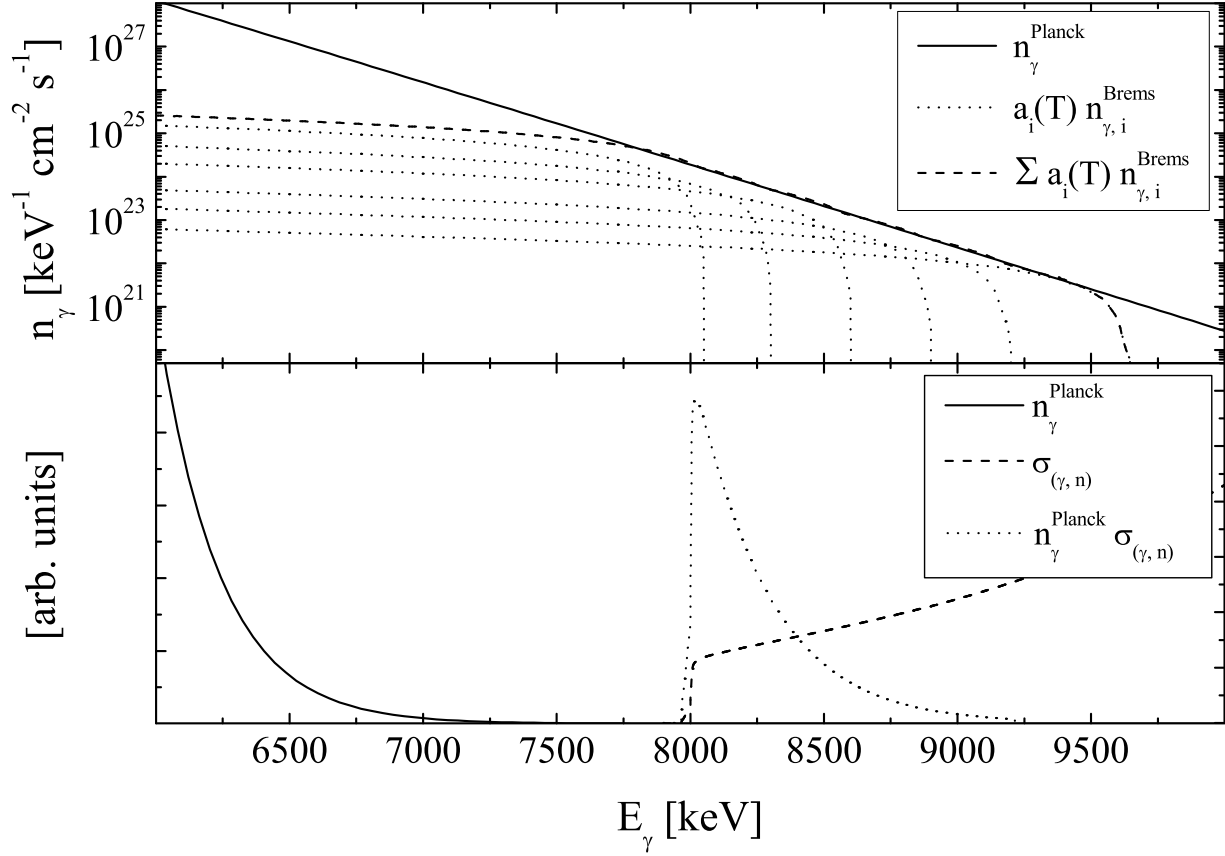


FIG. 9: The top panel shows a thermal Planck spectrum at $T = 2.5 \times 10^9$ K. The weighted sum of different bremsstrahlung spectra yields a good approximation of the Planck spectrum within the Gamow-like window. The bottom panel shows that this energy region is defined by the product of photon flux $n_{\gamma}^{\text{Planck}}$ and photoneutron cross section $\sigma_{(\gamma,n)}$ [21]. In this figure $\sigma_{(\gamma,n)}$ was calculated with the NON-SMOKER^{WEB} code [20] for the case of ^{154}Sm .

γ -ray strength function.

To compare the results of both predictions we used the default input parameters recommended by the authors of the codes. These input parameters are mainly intended to provide a global description for a wide range of isotopes. The NON-SMOKER^{WEB} code involves the neutron optical potential published by Jeukenne *et al.* [23] with a low-energy modification by Lejeune [24]. The γ -ray strength function is based on a description of Thielemann and Arnould [25] using experimental GDR energies and widths if available and the low-energy modification of the GDR Lorentzian by McCullagh *et al.* [26]. For the nuclear level density a global parametrization within the back-shifted Fermi-gas formalism by Rauscher *et al.* [27]

is applied. The TALYS code uses the neutron optical model potential parameterizations of Koning and Delaroche [28]. The γ -ray strength function is obtained from the compilation by Kopecky and Uhl [29] and the nuclear level density is also based on an approach using the Fermi-gas model [30]. Both the TALYS code and the NON-SMOKER^{WEB} code employ the Constant Temperature Model from Gilbert and Cameron [31] for the nuclear level density to avoid the divergence of the Fermi-gas model at low excitation energies.

The experimentally determined normalization factors f of these calculations for different energies E_{max} are presented in Fig. 10 and the results are summarized in Tab. II. Both statistical model codes are in fair agreement with our experimental data points. A χ^2 -test confirmed that the normalization factors derived for each isotope can be assumed to be independent of the energy E_{max} within the experimental uncertainties. For the absolute values of the cross sections we found a mean deviation of 24% and 27% between theory and experiment and a mean normalization factor f of 0.82 and 0.73 for the NON-SMOKER^{WEB} and the TALYS calculation, respectively. Thus, the predictions seem to slightly overestimate the photoneutron cross sections in the rare earth region.

The quoted uncertainties Δf_{sys} and Δf_{fit} denote the systematic and statistical uncertainties of the measurement, respectively. They are discussed in more detail in Sec. IV C. Δf_{fit} was derived from averaging the normalization factors f measured at different energies E_{max} with regard to the statistical uncertainties of each individual data point. The total uncertainty Δf_{total} is calculated by a Gaussian error propagation of Δf_{sys} and Δf_{fit} . Although the experimental uncertainty is about 20%, it has to be pointed out that most of the isotopes were simultaneously irradiated. Hence, systematic uncertainties are significantly reduced when comparing the normalization factors of these isotopes relative to each other. Therefore, the discrepancy between experimental data and theory cannot only be due to experimental uncertainties.

Figure 11 shows results from various experiments for the photoneutron cross section in the energy region of the giant dipole resonance. These data have been obtained by using several experimental techniques like absorption and activation measurements using bremsstrahlung, but also direct measurements of the energy dependence of the cross section using a quasi-monoenergetic photon beam produced by the annihilation in flight of monoenergetic positrons. Details of these experiments are given in [32, 33, 34, 35, 36, 37]. The theoretical predictions for the photoneutron cross sections normalized with the factors

found in our experiment have been compared to these data. For the isotopes ^{148}Nd , ^{154}Sm , and ^{160}Gd the normalized calculations appear to be slightly below the experimental data points, but are still fully consistent with these data points within the quoted uncertainties of the derived normalization factors. Furthermore, larger deviations have been found for ^{150}Nd and ^{154}Gd . Unfortunately, in the case of ^{150}Nd a comparison close to the neutron emission threshold is not possible, since no experimental data is available in this energy region. For ^{154}Gd a non-negligible photoneutron cross section was even stated below the neutron separation energy of $S_n = 8894.8$ keV in [34]. This indicates systematic uncertainties of these experimental data and might explain the discrepancy to the normalized predictions of this work.

Isotope	TALYS				NON-SMOKER ^{WEB}			
	f	Δf_{total}	Δf_{fit}	Δf_{sys}	f	Δf_{total}	Δf_{fit}	Δf_{sys}
^{148}Nd	0.86	0.176	0.052	0.169	0.86	0.176	0.052	0.169
^{150}Nd	0.55	0.111	0.037	0.105	0.62	0.127	0.047	0.118
^{154}Gd	0.55	0.102	0.052	0.088	0.56	0.100	0.045	0.090
^{160}Gd	0.93	0.151	0.039	0.145	1.15	0.186	0.051	0.179
^{154}Sm	0.74	0.119	0.029	0.115	0.89	0.143	0.034	0.139

TABLE II: Normalization factors derived from the experimental data for the theoretical predictions of the photoneutron cross section using the TALYS and NON-SMOKER^{WEB} code. The uncertainties Δf_{fit} and Δf_{sys} are discussed in detail in the text. Δf_{total} denotes the total experimental uncertainty derived from a Gaussian error propagation of Δf_{fit} and Δf_{sys} .

B. Determination of ground-state reaction rates

We have derived the (γ, n) ground-state reaction rates for $^{148,150}\text{Nd}$, ^{154}Gd , and ^{154}Sm at temperatures between 2 and 3×10^9 K using the approximation of a thermal Planck spectrum as described in Sec. III B. The results are presented in Tab. III.

The experimental uncertainties $\Delta \lambda_{\text{Exp, Yield}}^{\text{g.s.}}$ and $\Delta \lambda_{\text{Exp, Approx}}^{\text{g.s.}}$ stem from the experimental uncertainty of the reaction yield determination and from the uncertainty of the approximated

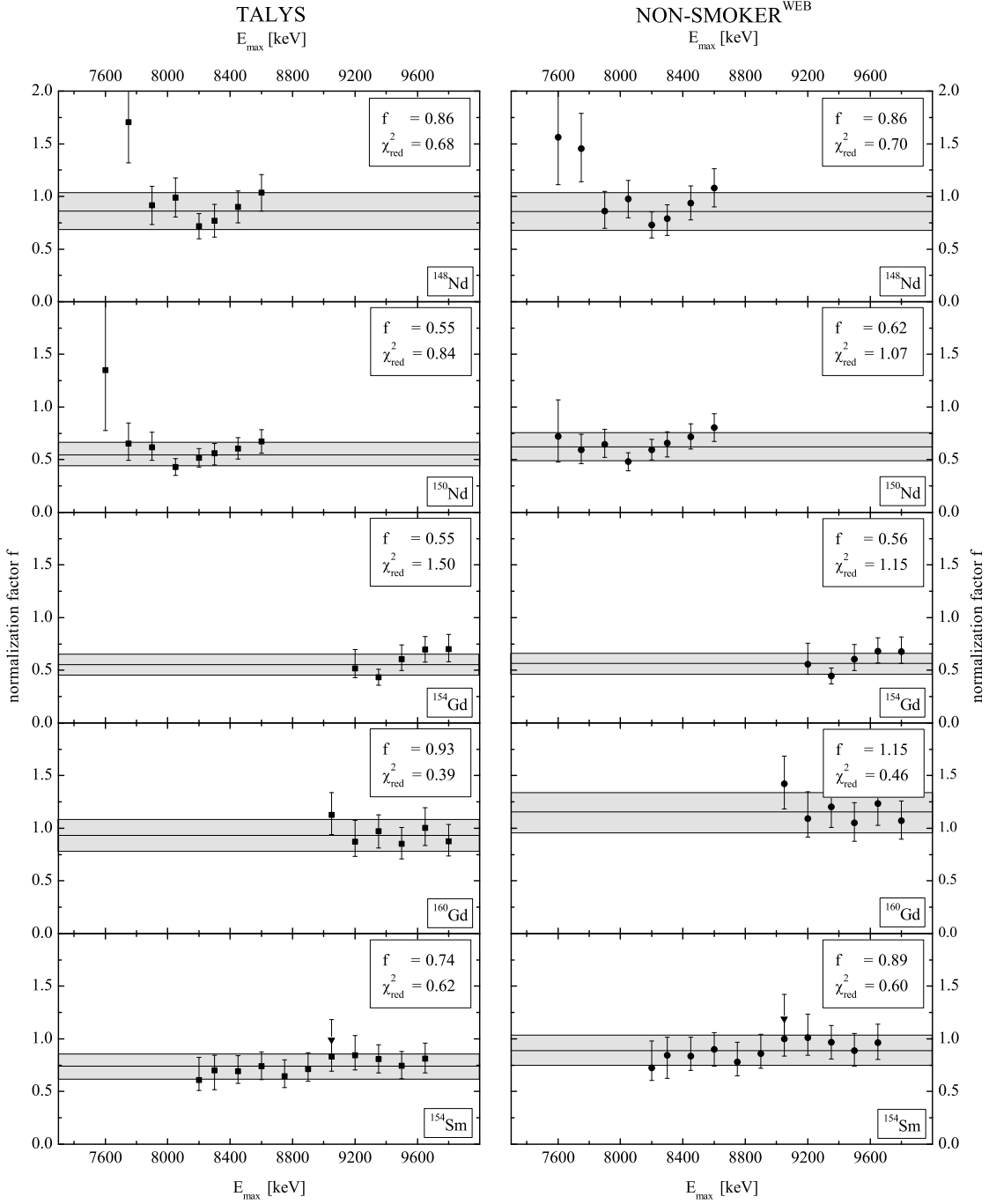


FIG. 10: Normalization factors f derived for two different theoretical predictions of the photoneutron cross section at various energies E_{max} . The grey error band denotes the experimental uncertainty Δf_{total} discussed in the text. The triangular data points at $E_{\text{max}} = 9050$ keV for ^{154}Sm are independent remeasurements to test the reproducibility of our experimental results.

	^{148}Nd	^{150}Nd	^{154}Gd	^{154}Sm
$T = 2.0 \times 10^9 \text{ K}$				
Upper energy limit	8380	8440	9850	8930
$\lambda_{\text{Exp}}^{\text{g.s.}}$	$5.97 \cdot 10^{-3}$	$3.52 \cdot 10^{-3}$	$2.74 \cdot 10^{-6}$	$4.78 \cdot 10^{-4}$
$\Delta\lambda_{\text{Exp,Yield}}^{\text{g.s.}}$	$1.10 \cdot 10^{-3}$	$0.64 \cdot 10^{-3}$	$0.50 \cdot 10^{-6}$	$0.85 \cdot 10^{-4}$
$\Delta\lambda_{\text{Exp,Approx}}^{\text{g.s.}}$	$1.64 \cdot 10^{-3}$	$0.85 \cdot 10^{-3}$	$0.48 \cdot 10^{-6}$	$0.54 \cdot 10^{-4}$
$\lambda_{\text{TALYS}}^{\text{g.s.}}$	$1.09 \cdot 10^{-2}$	$9.10 \cdot 10^{-3}$	$5.10 \cdot 10^{-6}$	$7.87 \cdot 10^{-4}$
$\lambda_{\text{N.S.}}^{\text{g.s.}}$	$1.20 \cdot 10^{-2}$	$9.44 \cdot 10^{-3}$	$5.01 \cdot 10^{-6}$	$6.53 \cdot 10^{-4}$
$T = 2.5 \times 10^9 \text{ K}$				
Upper energy limit	8655	8715	10120	9205
$\lambda_{\text{Exp}}^{\text{g.s.}}$	$6.45 \cdot 10^1$	$4.09 \cdot 10^1$	$1.12 \cdot 10^{-1}$	$7.45 \cdot 10^0$
$\Delta\lambda_{\text{Exp,Yield}}^{\text{g.s.}}$	$1.17 \cdot 10^1$	$0.74 \cdot 10^1$	$0.21 \cdot 10^{-1}$	$1.32 \cdot 10^0$
$\Delta\lambda_{\text{Exp,Approx}}^{\text{g.s.}}$	$1.39 \cdot 10^1$	$0.99 \cdot 10^1$	$0.34 \cdot 10^{-1}$	$0.46 \cdot 10^0$
$\lambda_{\text{TALYS}}^{\text{g.s.}}$	$8.19 \cdot 10^1$	$7.74 \cdot 10^1$	$2.07 \cdot 10^{-1}$	$1.11 \cdot 10^1$
$\lambda_{\text{N.S.}}^{\text{g.s.}}$	$8.62 \cdot 10^1$	$7.16 \cdot 10^1$	$2.06 \cdot 10^{-1}$	$9.21 \cdot 10^0$
$T = 3.0 \times 10^9 \text{ K}$				
Upper energy limit	8945	9010	10400	9505
$\lambda_{\text{Exp}}^{\text{g.s.}}$	$2.92 \cdot 10^4$	$1.78 \cdot 10^4$	$1.49 \cdot 10^2$	$5.04 \cdot 10^3$
$\Delta\lambda_{\text{Exp,Yield}}^{\text{g.s.}}$	$0.54 \cdot 10^4$	$0.33 \cdot 10^4$	$0.29 \cdot 10^2$	$0.88 \cdot 10^3$
$\Delta\lambda_{\text{Exp,Approx}}^{\text{g.s.}}$	$0.99 \cdot 10^4$	$0.67 \cdot 10^4$	$0.52 \cdot 10^2$	$0.28 \cdot 10^3$
$\lambda_{\text{TALYS}}^{\text{g.s.}}$	$3.31 \cdot 10^4$	$3.25 \cdot 10^4$	$2.58 \cdot 10^2$	$6.79 \cdot 10^3$
$\lambda_{\text{N.S.}}^{\text{g.s.}}$	$3.39 \cdot 10^4$	$2.91 \cdot 10^4$	$2.58 \cdot 10^2$	$5.65 \cdot 10^3$

TABLE III: The ground-state reaction rates (in s^{-1}) determined experimentally by the approximation approach of a thermal Planck spectrum for three different temperatures are in good agreement with two theoretical predictions using the TALYS and NON-SMOKER^{WEB} code. The energy range between the neutron emission threshold energy and the quoted upper energy limit (in keV) is estimated to contribute about 99% to the total ground-state reaction rate. $\Delta\lambda_{\text{Exp,Yield}}^{\text{g.s.}}$ and $\Delta\lambda_{\text{Exp,Approx}}^{\text{g.s.}}$ account for the uncertainty of the experimental reaction yield and for the uncer-

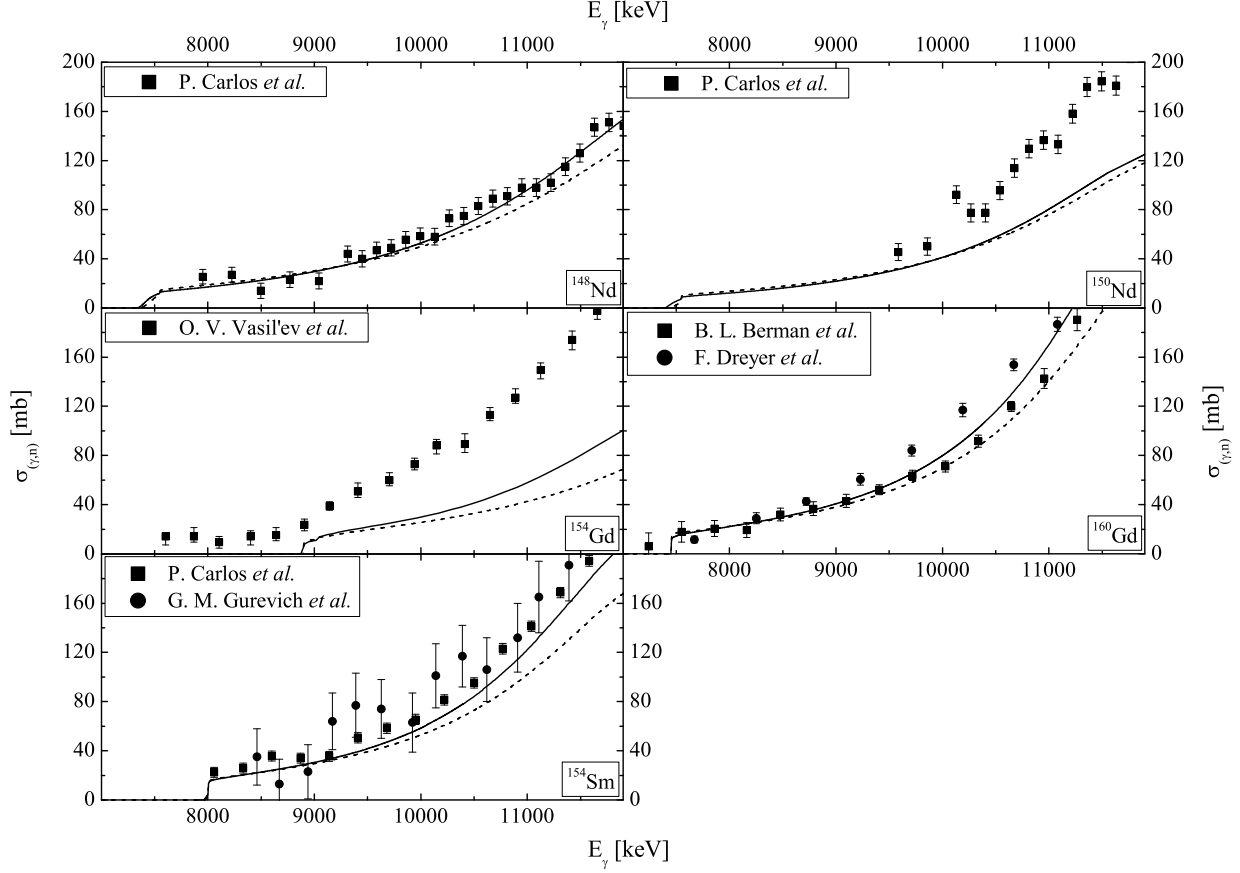


FIG. 11: Comparison of experimental data for the photoneutron cross section from various photodisintegration experiments [32, 33, 34, 35, 36, 37] and theoretical predictions using the TALYS (dashed line) and NON-SMOKER^{WEB} code (solid line). The theoretical calculations were normalized with the factors presented in Tab. II. Note that the error bands of the theoretical predictions due to the experimental uncertainties of the applied normalization factors have been omitted in the graphs.

thermal Planck spectrum within the Gamow-like window, respectively. As will be discussed in Sec. IV C, the experimental data points close to the neutron emission threshold suffer from large uncertainties. Hence, we discarded these data points for the analysis to increase the reliability of the experimental determination of the ground-state reaction rates, although the approximation of the Planck spectrum, therefore, became less accurate. Moreover, for the isotopes $^{148,150}\text{Nd}$ and ^{154}Gd experimental data points were missing at energies further above the neutron separation energy. This also reduced the accuracy of the approximation of the Planck spectra at temperatures close to 3×10^9 K. Thus, except for the case of ^{154}Sm

the approximation in this experiment was less accurate than stated in Sec. III B. For ^{160}Gd too few data points were available in the energy region of interest to derive ground-state reaction rates using the approximation approach.

For comparison the ground-state reaction rates were calculated from Eq. (5) using the unnormalized theoretical predictions for the photoneutron cross sections discussed in the preceding section. As shown in Tab. III the calculations are in good agreement with the experimental results within the experimental uncertainties and the uncertainties of the approximation. Consistent with the results found for the normalization factors of the photoneutron cross section the statistical model calculations tend to slightly overestimate the reaction rates for the studied isotopes.

C. Discussion of systematic and statistical uncertainties

An overview of the various experimental uncertainties is shown in Tab. IV. We distinguish between systematic uncertainties Δ_{sys} and statistical uncertainties Δ_{stat} . The latter are not correlated between the different experimental runs at various energies E_{max} and can, therefore, be reduced by a large number of individual measurements. The contribution of the various uncertainties to the overall uncertainty will be discussed in detail in the following.

The dominant uncertainty in our experiment comes from the determination of the photon flux as discussed in Sec. II A. The systematic uncertainty Δ_{sys} denotes the mean deviation between the normalized GEANT4 simulation and the experimental data points stemming from the photoscattering reaction $^{11}\text{B}(\gamma, \gamma')$. Therefore, Δ_{sys} describes the uncertainty of the determined spectral distribution of the photon flux. In addition Δ_{stat} accounts for the statistical uncertainties of the $^{11}\text{B}(\gamma, \gamma')$ reaction yields used for the normalization of the simulation.

Close to the neutron emission threshold the reaction yield is highly dependent on the maximum photon energy E_{max} of the activation. Thus, small uncertainties of E_{max} close to the neutron emission threshold give rise to large uncertainties in the cross section determination as illustrated in Fig. 12. For our analysis we estimated E_{max} to be known with an uncertainty of 25 keV. We assumed that there was no systematic deviation of E_{max} inherent to all experimental runs and, hence, no systematic uncertainty was taken into account. Therefore, the uncertainty of E_{max} was only treated statistically in the analysis.

	Δ_{sys}	Δ_{stat}
photon flux	16%	5%
E_{max}	—	*
detection efficiency	4%	2% [†] / 15% [‡]
self-absorption	5%	—
counting	—	2%
γ -intensity	3%	—
target mass	—	2%
total	18%	6% [†] / 16% [‡]

TABLE IV: Systematic and statistical uncertainties of the determination of the experimental (γ, n) reaction yield. The two uncertainties of the detection efficiency stated refer to the HPGe setup ([†]) and the LEPS setup ([‡]), respectively. The uncertainties stemming from an uncertainty in the maximum photon energy E_{max} (*) are illustrated in Fig. 12. The total uncertainty is calculated by a Gaussian error propagation.

Due to averaging over many individual measurements at various E_{max} , the uncertainty of E_{max} only represents a minor contribution of the order of a few percent to the total uncertainty of the determined normalization factors.

To derive the reaction yield from the measured activities of the produced unstable isotopes the detection efficiency has to be known accurately. As already discussed in Sec. II B the detection efficiency was determined with an uncertainty of 7%. Since each reaction yield was derived from several γ -transitions of different energies the average systematic uncertainty was reduced to about 4%. Besides, it was found that the observed activation count rate very sensitively depended on a proper placement of the target in front of the detectors. Repeated measurements with calibration sources showed that an additional uncertainty of 2% at the HPGe setup and, due to the very short distance between target and detector, an uncertainty of 15% at the LEPS setup had to be taken into account. These measurements also proved that this uncertainty could be treated statistically, and, hence, was reduced by averaging over many data points.

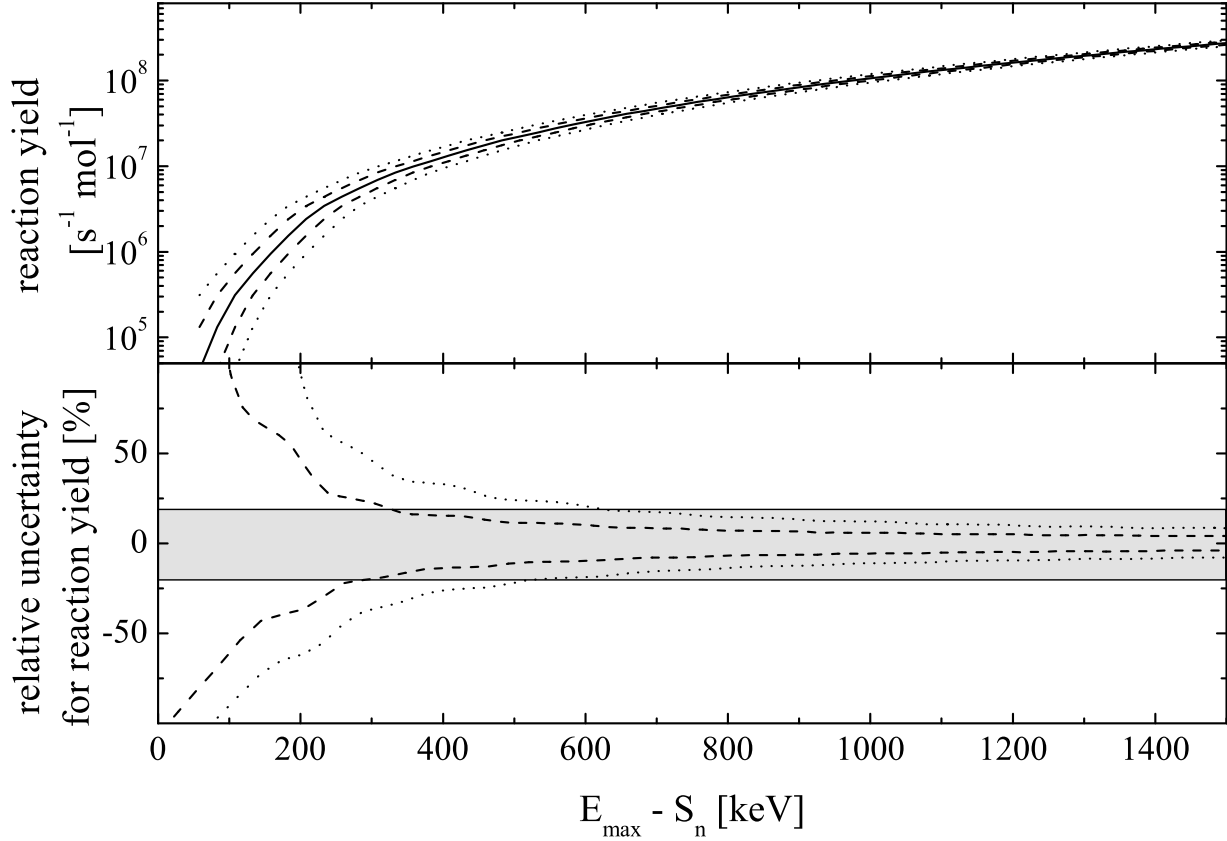


FIG. 12: The expected (γ, n) reaction yield of a ^{154}Sm target (top panel) using a NON-SMOKER^{WEB} calculation for the photoneutron cross section (solid line). The dashed and dotted lines indicate the error bands assuming uncertainties of E_{max} of 25 keV and 50 keV, respectively. The bottom panel shows that close to the neutron threshold this uncertainty clearly dominates the uncertainty stemming from the photon flux determination (grey band).

Other uncertainties stemming from the self-absorption of emitted photons within the target, the statistical uncertainty of the counting, the γ -intensities of the decays and the target mass were typical of the order of a few percent.

The total experimental uncertainty derived from the various contributions discussed in this section is stated in Tab. IV. As can be seen, the accuracy is mainly limited by systematic uncertainties. Nevertheless, one also has to account for large statistical uncertainties, when the reaction yield is determined for a single experimental run. However, the statistical uncertainties are significantly reduced when averaging over many data points in the analysis as done for the deduction of the normalization factors and ground-state reactions rates.

Therefore, the total experimental uncertainties for the results presented in this work are typical of the order of 20%.

V. SUMMARY AND CONCLUSION

In the last years extensive studies of photoneutron reactions with astrophysical implication for isotopes in the mass region $A \geq 186$ have been carried out, but no experimental data have been provided for the rare earth isotopes so far. However, reliable experimental data for a wide range of isotopes in various mass regions are mandatory in order to constrain and to improve the theoretical calculations required for astrophysical reaction networks. The intention of this work was to test the theoretical predictions of two different statistical model codes for the photoneutron cross sections and ground-state reaction rates in the rare earth region. Although a variety of photoneutron reactions in this mass region was studied in the 70s, these experiments mainly focused on the investigation of the Giant Dipole Resonance. Hence, data points stemming from these experiments usually underlie large statistical and systematical uncertainties close to the neutron threshold and do not serve as a reliable test for theoretical predictions in the astrophysically relevant energy region. Therefore, we determined normalization factors for the calculations of the photoneutron cross sections of the isotopes $^{148,150}\text{Nd}$, ^{154}Sm , and $^{154,160}\text{Gd}$ in photoactivation experiments close to the neutron separation energy. Moreover, we derived (γ, n) ground-state reaction rates in the astrophysically relevant energy region for the p process using a superposition of bremsstrahlung spectra of various energies.

The need of experimental data of photoneutron reactions for astrophysical reaction networks is twofold. First, for p -process studies reliable predictions of reaction rates for a wide range of isotopes need to be provided. Since most of the isotopes involved in the p -process reaction network are unstable, the nuclear physics input for these isotopes is rare and, hence, theoretical calculations usually cannot be adjusted locally. Therefore, the reliability of the theoretical models should be tested using only global input parameters. In this work we found that in the rare earth region the predicted cross sections and the reaction rates for the selected isotopes agree with the experimental data within a factor of two. On average, a mean uncertainty of less than 30% has been determined. This is consistent with the results found in previous experiments in the mass region $A \geq 186$. In addition, no systematic

dependence of the deviation with atomic mass has been observed. On the one hand, this proves the reliability of the statistical model codes for a wide range of isotopes along the valley of stability. But it also indicates an appropriate predictive power for the reaction rates of unstable isotopes, since only global input parameters were used in the calculations. However, for almost all studied isotopes the cross sections were found to be overestimated by theory, which calls for further investigations. Moreover, it is planned to study the isotopic chain of the cerium isotopes in the near future to test the validity of the statistical model in this mass region for isotopes close to and at the neutron shell closure. Although the predictions agree fairly well with the experimental data of this work, it needs to be emphasized that experimental studies cannot account for the stellar enhancement of cross sections and reaction rates due to the thermal population of low-lying levels in the parent nuclei under stellar conditions. This so-called *stellar enhancement factor* can only be derived from theory.

The second astrophysical application of experimental studies of photoneutron reactions arises in the investigation of branching points within the *s* process. In this context the photoneutron reactions of ^{148}Nd and ^{154}Gd are of particular interest among the studied isotopes of this work. Since the neighbouring branching points ^{147}Nd and ^{153}Gd cannot be studied in neutron capture experiments due to their short half-life, the aim is to derive the neutron capture cross sections of these branching points from the photoneutron reaction of the isotopes ^{148}Nd and ^{154}Gd , respectively. It was shown in this work, that the two adopted theoretical predictions overestimate the photoneutron cross sections by up to a factor of two. This might indicate that also the predicted neutron capture cross section of the inverse reactions need to be adjusted accordingly when being calculated within the same statistical model code. For astrophysical studies, a direct correlation between the stellar neutron capture and photodisintegration rate is described by the so-called *principle of detailed balance* [38, 39]. This correlation only holds under the assumption that the low-lying levels in both the parent and the residual nucleus are thermally populated to a significant amount. This condition is fulfilled under sufficiently hot temperatures in a stellar environment. However, experiments in the laboratory only address transitions starting from the ground state of a certain nucleus and, therefore, the principle of detailed balance is not applicable any more for a direct comparison of the laboratory neutron capture and photodisintegration rate. Hence, without any further assumptions, conclusions for the neutron capture rate can hardly be drawn from

the reaction rates derived in photodisintegration experiments.

Instead of directly deriving the neutron capture reaction rate from experiment a promising approach is to improve the nuclear physics input of the statistical model codes in order to increase the reliability of the theoretical predictions. To obtain the most accurate calculations for a single nucleus the input parameters should be adjusted locally. Therefore, the aim of future studies should be to provide improved nuclear physics input for ^{148}Nd and ^{154}Gd , while the experimental results of this work serve as a reliable test for any new complete set of input parameters. It can be assumed that a set of input parameters yielding improved predictions for the photoneutron reaction, will then also enhance the calculations of the neutron capture cross sections of the branching points ^{147}Nd and ^{153}Gd . At this point, however, we would like to make clear that the experimental data provided by this work set constraints on the absolute value of the photoneutron cross section, but do not allow for separately adjusting the various nuclear physics parameters such as the neutron optical potential, nuclear level densities and the γ -ray strength function. Therefore, further experimental investigations with direct access to these parameters are mandatory in the future.

VI. ACKNOWLEDGMENTS

We thank the S-DALINAC group around R. Eichhorn for the reliable beam during our experiment and T. Rauscher for his support with the theoretical calculations using the NON-SMOKER^{WEB} code. Moreover, we thank the Karlsruhe group around F. Käppeler for helping us with the target preparation. This work was supported by the Deutsche Forschungsgemeinschaft under contract SFB 634.

-
- [1] D. L. Lambert, *Astron. Astroph. Rev.* **3**, 201 (1992).
- [2] M. Arnould and S. Goriely, *Phys. Rep.* **384**, 1 (2003).
- [3] Z. Y. Bao, H. Beer, F. Käppeler, F. Voss, K. Wisshak, and T. Rauscher, *At. Data Nucl. Data Tables* **76**, 70 (2000).
- [4] KADONIS - Karlsruhe Astrophysical Database of Nucleosynthesis in Stars,
<http://nuclear-astrophysics.fzk.de/kadonis/>.
- [5] F. Käppeler and A. Mengoni, *Nucl. Phys.* **A777**, 291 (2006).
- [6] K. Sonnabend, P. Mohr, K. Vogt, A. Zilges, A. Mengoni, T. Rauscher, H. Beer, F. Käppeler, and R. Gallino, *Astrophys. J.* **583**, 506 (2003).
- [7] K. Vogt, P. Mohr, M. Babilon, J. Enders, T. Hartmann, C. Hutter, T. Rauscher, S. Volz, and A. Zilges, *Phys. Rev. C* **63**, 055802 (2001).
- [8] K. Vogt, P. Mohr, M. Babilon, W. Bayer, D. Galaviz, T. Hartmann, C. Hutter, T. Rauscher, K. Sonnabend, S. Volz, et al., *Nucl. Phys.* **A707**, 241 (2002).
- [9] K. Sonnabend, K. Vogt, D. Galaviz, S. Müller, and A. Zilges, *Phys. Rev. C* **70**, 035802 (2004).
- [10] S. Müller, A. Kretschmer, K. Sonnabend, A. Zilges, and D. Galaviz, *Phys. Rev. C* **73**, 025804 (2006).
- [11] E. Anders and N. Grevesse, *Geochim. Cosmochim. Acta* **53**, 197 (1989).
- [12] S. Jaag and F. Käppeler, *Phys. Rev. C* **51**, 3465 (1995).
- [13] R. Reifarth, C. Arlandini, M. Heil, F. Käppeler, P. V. Sedyshev, A. Mengoni, M. Herman, T. Rauscher, and R. Gallino, *Astrophys. J.* **582**, 1251 (2003).
- [14] K. Wisshak, R. Gallino, F. Käppeler, M. Krücka, A. Mengoni, S. Raman, and F. Voss, *Phys. Rev. C* **73**, 015802 (2006).
- [15] S. Marrone, U. Abbondanno, G. Aerts, F. Alvarez-Velarde, H. Alvarez-Pol, S. Andriamonje, J. Andrzejewski, G. Badurek, P. Baumann, F. Becvar, et al., *Phys. Rev. C* **73**, 034604 (2006).
- [16] A. Richter, in *Proceedings of Fifth European Particle Accelerator Conference*, edited by S. Meyers, A. Pacheco, R. Pascual, C. Petit-Jean-Genaz, and J. Poole (IOP, Bristol, 1996), p. 110.
- [17] revision of August 2, 2006, NNDC Online Data Service, ENSDF database,
<http://www.nndc.bnl.gov/nndc/ensdf/> (2006).
- [18] S. Agostinelli, J. Allison, K. Amako, J. Apostolakis, H. Araujo, P. Arce, M. Asai, D. Axen,

- S. Banerjee, G. Barrand, et al., Nucl. Instr. and Meth. A **506**, 250 (2003).
- [19] GEANT, Application Software Group, GEANT 3.21, CERN programm Library Long Writeup **W5013** (1994).
- [20] NON-SMOKER^{WEB}, last updated 26th of August 2006,
<http://nucastro.org/nonsmoker.html>.
- [21] P. Mohr, K. Vogt, M. Babilon, J. Enders, T. Hartmann, C. Hutter, T. Rauscher, S. Volz, and A. Zilges, Phys. Lett. B **488**, 127 (2000).
- [22] A. J. Koning, S. Hilaire, and M. C. Duijvestijn, in *Proceedings of the International Conference on Nuclear Data for Science and Technology - ND2004, Sep. 26 - Oct. 1, 2004, Santa Fe, USA*, edited by R. C. Haight, M. B. Chadwick, T. Kawano, and P. Talou (2005), vol. 769 of *AIP*, p. 1154.
- [23] J.-P. Jeukenne, A. Lejeune, and C. Mahaux, Phys. Rev. C **16**, 80 (1977).
- [24] A. Lejeune, Phys. Rev. C **21**, 1107 (1980).
- [25] F.-K. Thielemann and M. Arnould, in *Proceedings of the International Conference on Nuclear Data for Science and Technology*, edited by K. Böckhoff (D. Reidel Publ. Co., Brüssel, 1983), p. 762.
- [26] C. M. McCullagh, M. L. Stelts, and R. E. Chrien, Phys. Rev. C **23**, 1394 (1981).
- [27] T. Rauscher, F.-K. Thielemann, and K.-L. Kratz, Phys. Rev. C **56**, 1613 (1997).
- [28] A. J. Koning and J. P. Delaroche, Nucl. Phys. **A713**, 231 (2003).
- [29] J. Kopecky and M. Uhl, Phys. Rev. C **41**, 1941 (1990).
- [30] T. Ericson, Adv. Phys. **9**, 425 (1960).
- [31] A. Gilbert and A. G. W. Cameron, Can. J. Phys. **43**, 1446 (1965).
- [32] P. Carlos, H. Beil, R. Bergère, A. Leprêtre, and A. Veyssière, Nucl. Phys. **A172**, 437 (1971).
- [33] P. Carlos, H. Beil, R. Bergère, A. Leprêtre, and A. de Miniac, Nucl. Phys. **A225**, 171 (1974).
- [34] O. V. Vasil'ev, V. A. Semenov, and S. F. Semenko, Yad. Fiz. **13**, 463 (1971).
- [35] G. M. Gurevich, L. E. Lazareva, V. M. Mazur, S. Y. Merkulov, G. V. Solodukhov, and V. A. Tyutin, Nucl. Phys. **A351**, 257 (1981).
- [36] F. Dreyer, H. Dahmen, J. Staude, and H. H. Thies, Nucl. Phys. **A192**, 433 (1972).
- [37] B. L. Berman, M. A. Kelly, R. L. Bramblett, J. T. Caldwell, H. S. Davis, and S. C. Fultz, Phys. Rev. **185**, 1576 (1969).
- [38] W. A. Fowler, G. E. Caughlan, and B. A. Zimmermann, Annu. Rev. Astron. Astrophys. **5**,

525 (1967).

[39] T. Rauscher and F.-K. Thielemann, *At. Data Nucl. Data Tables* **75**, 1 (2000).